

Dynamical classicalization

J. Rizos⁽¹⁾ and N. Tetradis⁽²⁾

(1) Theory Division, Department of Physics, University of Ioannina, Ioannina 45110, Greece

(2) Department of Physics, University of Athens, University Campus, Zographou 15784, Greece

We integrate numerically the nonlinear equation of motion for a collapsing spherical wavepacket in the context of theories that are expected to display behavior characteristic of classicalization. The classicalization radius sets the scale for the onset of significant deformations of the collapsing configuration, which result in the formation of shock fronts. A characteristic observable feature of the classicalization process is the creation of an outgoing field configuration that extends far beyond the classicalization radius. This feature develops before the deformed wavepacket reaches distances of the order of the fundamental scale. We find that in some models the scattering problem may not have real solutions over the whole space at late times. We determine the origin of this behavior and discuss the consistency of the underlying models.

1. INTRODUCTION

The physics of classicalization concerns the nature of high-energy scattering in certain classes of nonrenormalizable field theories. The proposal of refs. [1–4] is that scattering can take place at length scales much larger than the typical scale associated with the nonrenormalizable terms in the Lagrangian. The behavior is similar to ultra-Planckian scattering in gravitational theories, during which a black hole is expected to start forming at distances comparable to the Schwarzschild radius. For sufficiently large center-of-mass energy, the Schwarzschild radius can be much larger than the Planck length. If the formation and subsequent evaporation of a black hole are viewed as parts of a scattering process, it becomes clear that the physical length scale determining the cross section can be the Schwarzschild radius and not the Planck scale. It has been advocated that similar behavior may be observed in some nonrenormalizable field theories [1–4]. In scattering processes, the center-of-mass energy introduces a new dimensionful scale in the problem that can be used to define the analogue of the Schwarzschild radius. This new length scale is termed classicalization radius. It defines the distance at which scattering starts and, for sufficiently high center-of-mass energy, can be much larger than the fundamental length scale L_* of the theory, determined by the coefficient of the non-renormalizable term in the action. The scenario has very interesting collider phenomenology [5].

An idealized scattering process was proposed in refs. [2, 3] as a means to check the validity of the classicalization arguments. The process involves an initial spherical wavepacket of very large radius that propagates towards the center of symmetry. The solution of the classical equation of motion can provide a clear indication of the onset of scattering. One expects that it should be possible to verify that this starts at length scales much larger than L_* . An approximate analytical solution of the equation of motion was presented in refs. [2, 3]. It demonstrates that there are significant corrections to the initial wavepacket at length scales of order r_* , with the simultaneous creation of a long tail in the field configuration, stretching out to large distances. However, an exact solution of the equation of motion is still lacking. In ref. [6], it was suggested that the equation of motion can be written as a quasi-linear partial differential equation of second order. For the initial spherical wavepacket this equation is hyperbolic, supporting the propagation of wavelike configurations. However, when the center of the wavepacket approaches r_* , the equation may become elliptic in certain regions. This change could result in the suppression of wave propagation and the emergence of scattering.

In this work we present numerical solutions of the field equations of motion for two theories, described by nonrenormalizable Lagrangians, which are expected to generate behavior characteristic of classicalization. We discuss in detail how the typical features of classicalization emerge during the evolution of the idealized spherical wavepacket described above. We also point out several novel features that seem to be inherent in scattering processes in the context of such theories. In the following two sections we describe the theories in question. In section 4 we present the method we employ for the integration of the equations of motion. We also discuss the crucial issue of existence or absence of real solutions in certain ranges of the radial coordinate r . In section 5 we present the results of the numerical integration. In the final section we discuss the interpretation of our results.

2. QUARTIC ACTION

The prototype scalar theory in which classicalization is expected to occur is described by the Lagrangian density

$$\mathcal{L} = \frac{1}{2} (\partial_\mu \phi)^2 - \delta_1 \frac{L_*^4}{4} \left((\partial_\mu \phi)^2 \right)^2. \quad (1)$$

We allow for both signs of the higher derivative term by assuming that δ_1 can take the values $\delta_1 = \pm 1$. The equation of motion of the field ϕ is

$$\partial^\mu \left[\partial_\mu \phi \left(1 - \delta_1 L_*^4 (\partial_\nu \phi)^2 \right) \right] = 0. \quad (2)$$

An idealized scattering process, which displays the characteristic behavior associated with classicalization, involves a collapsing spherical wavepacket initially represented by a Gaussian of width a centered around a radius r_0 . It has the form

$$\phi_0(t, r) = \frac{A}{r} \exp \left[-\frac{(r + t - r_0)^2}{a^2} \right]. \quad (3)$$

Using perturbation theory, it was shown in refs. [2, 3] that the field configuration is strongly deformed when the peak of the wavepacket reaches the classicalization radius

$$r_* \sim L_* \left(\frac{A^2 L_*}{a} \right)^{1/3}. \quad (4)$$

This can be substantially larger than the fundamental length scale L_* when the center-of-mass energy $s \sim A^2/a$ is much larger than $1/L_*$. It must be noted that the analysis of refs. [2, 3] was carried out for the case $\delta_1 = -1$. However, it is straightforward to check that the same arguments apply to the case $\delta_1 = 1$ as well.

Another point of view was presented in ref. [6]. It was argued that the behavior associated with classicalization is related to the dynamical change of type of the classical equation of motion. For a spherically symmetric configuration, eq. (2) takes the form

$$(1 - 3\lambda\phi_t^2 + \lambda\phi_r^2) \phi_{tt} - (1 - \lambda\phi_t^2 + 3\lambda\phi_r^2) \phi_{rr} + 4\lambda\phi_r \phi_t \phi_{tr} = \frac{2\phi_r}{r} (1 - \lambda\phi_t^2 + \lambda\phi_r^2), \quad (5)$$

where $\lambda = \delta_1 L_*^4$ and subscripts denote partial derivatives. The above equation can be expressed as a conservation law, in the form

$$\partial_t [\phi_t (1 - \lambda\phi_t^2 + \lambda\phi_r^2)] - \frac{1}{r^2} \partial_r [r^2 \phi_r (1 - \lambda\phi_t^2 + \lambda\phi_r^2)] = 0. \quad (6)$$

It can also be expressed as

$$\partial_t \left[\frac{1}{2} (\phi_t^2 + \phi_r^2) + \frac{\lambda}{4} (-3\phi_t^4 + \phi_r^4 + 2\phi_t^2 \phi_r^2) \right] - \frac{1}{r^2} \partial_r [r^2 \phi_t \phi_r (1 - \lambda\phi_t^2 + \lambda\phi_r^2)] = 0. \quad (7)$$

This last equation is equivalent to the conservation of the energy-momentum tensor resulting from the Lagrangian of eq. (1). The quantity

$$\rho = \frac{1}{2} (\phi_t^2 + \phi_r^2) + \frac{\lambda}{4} (-3\phi_t^4 + \phi_r^4 + 2\phi_t^2 \phi_r^2) \quad (8)$$

is the local energy density. The initial conditions for the solution of the equation of motion are of the Cauchy type:

$$\phi(0, r) = \phi_0(0, r), \quad \partial_t \phi(0, r) = \partial_t \phi_0(0, r), \quad (9)$$

where we assume that r_0 is much larger than any other physical scale.

The properties of eq. (5) become more transparent if it is written in the form of a quasilinear second-order partial differential equation:

$$\mathcal{A}(\phi_t, \phi_r) \phi_{tt} + \mathcal{B}(\phi_t, \phi_r) \phi_{tr} + \mathcal{C}(\phi_t, \phi_r) \phi_{rr} = \mathcal{D}(\phi_t, \phi_r, r), \quad (10)$$

with

$$\mathcal{A}(\phi_t, \phi_r) = 1 - 3\lambda\phi_t^2 + \lambda\phi_r^2 \quad (11)$$

$$\mathcal{B}(\phi_t, \phi_r) = 4\lambda\phi_t\phi_r \quad (12)$$

$$\mathcal{C}(\phi_t, \phi_r) = -(1 - \lambda\phi_t^2 + 3\lambda\phi_r^2) \quad (13)$$

$$\mathcal{D}(\phi_t, \phi_r, r) = \frac{2\phi_r}{r} (1 - \lambda\phi_t^2 + \lambda\phi_r^2). \quad (14)$$

The type of this partial differential equation is determined by the discriminant

$$\Delta = \frac{1}{4}(\mathcal{B}^2 - 4\mathcal{A}\mathcal{C}) = 3 \left(\frac{1}{3} - \lambda\phi_t^2 + \lambda\phi_r^2 \right) (1 - \lambda\phi_t^2 + \lambda\phi_r^2). \quad (15)$$

For $\Delta > 0$ the equation is hyperbolic, for $\Delta = 0$ parabolic, while for $\Delta < 0$ elliptic. Hyperbolic equations admit wave-like solutions, while elliptic ones do not support propagating solutions. The observation of ref. [6] is that classicalization may be associated with the change of the type of the equation during the evolution of the initial configuration. It can be shown [6] that, if \mathcal{A} , \mathcal{B} , \mathcal{C} are evaluated for the configuration (3), the discriminant (15) switches sign in a certain r -interval when the wavepacket moves into the vicinity of the classicalization radius (4). The sign change occurs for both values of δ_1 . As a result, we expect behavior associated with classicalization in both cases.

3. DIRAC-BORN-INFELD ACTION

A related theory, which can also display the classicalization phenomenon, is described by a Lagrangian density of the Dirac-Born-Infeld (DBI) type:

$$\mathcal{L} = -\frac{1}{\delta_2 L_*^4} \sqrt{1 - \delta_2 L_*^4 (\partial_\mu \phi)^2}, \quad (16)$$

with $\delta_2 = \pm 1$, as in the previous case. The equation of motion of the field ϕ is

$$\partial^\mu \left[\frac{\partial_\mu \phi}{\sqrt{1 - \delta_2 L_*^4 (\partial_\nu \phi)^2}} \right] = 0. \quad (17)$$

The leading terms in the expansion of the l.h.s. of the above equations reproduce the quartic model of the previous section, provided that we take $\delta_2 = -2\delta_1$. The Lagrangian (16) also includes a cosmological constant term, which is irrelevant for our considerations. In general, we expect similar behavior for the solutions of eqs. (2), (17) if δ_1 , δ_2 are taken with opposite signs. However, the higher-order terms resulting from the expansion of the l.h.s. of eq. (17) are also important for the dynamics.

When expressed in spherical coordinates, eq. (17) can be put in the form

$$(1 + \lambda\phi_r^2) \phi_{tt} - (1 - \lambda\phi_t^2) \phi_{rr} - 2\lambda\phi_r\phi_t \phi_{tr} = \frac{2\phi_r}{r} (1 - \lambda\phi_t^2 + \lambda\phi_r^2), \quad (18)$$

where $\lambda = \delta_2 L_*^4$ and subscripts denote partial derivatives. It is important to emphasize that, in order to obtain the above equation, eq. (17) must be multiplied by $(1 - \lambda\phi_t^2 + \lambda\phi_r^2)^{3/2}$. As a result, we must assume that

$$1 - \lambda\phi_t^2 + \lambda\phi_r^2 \geq 0. \quad (19)$$

This assumption is an obvious constraint imposed by the form of the Lagrangian density (16). Eq. (18) can also be expressed as a conservation law, in the form

$$\partial_t \left[\frac{\phi_t}{\sqrt{1 - \lambda\phi_t^2 + \lambda\phi_r^2}} \right] - \frac{1}{r^2} \partial_r \left[r^2 \frac{\phi_r}{\sqrt{1 - \lambda\phi_t^2 + \lambda\phi_r^2}} \right] = 0. \quad (20)$$

It can also be written in the form

$$\partial_t \left[\frac{1 + \lambda\phi_r^2}{\lambda\sqrt{1 - \lambda\phi_t^2 + \lambda\phi_r^2}} \right] - \frac{1}{r^2} \partial_r \left[r^2 \frac{\phi_r\phi_t}{\sqrt{1 - \lambda\phi_t^2 + \lambda\phi_r^2}} \right] = 0. \quad (21)$$

This last equation is equivalent to the conservation of the energy-momentum tensor resulting from the Lagrangian density of eq. (16). The quantity

$$\rho = \frac{1 + \lambda\phi_r^2}{\lambda\sqrt{1 - \lambda\phi_t^2 + \lambda\phi_r^2}} - \frac{1}{\lambda} \quad (22)$$

is the local energy density, after the subtraction of a cosmological constant included in the Lagrangian.

Eq. (18) can be written in the form (10) with

$$\mathcal{A}(\phi_t, \phi_r) = 1 + \lambda\phi_r^2 \quad (23)$$

$$\mathcal{B}(\phi_t, \phi_r) = -2\lambda\phi_t\phi_r \quad (24)$$

$$\mathcal{C}(\phi_t, \phi_r) = -(1 - \lambda\phi_t^2) \quad (25)$$

$$\mathcal{D}(\phi_t, \phi_r, r) = \frac{2\phi_r}{r} (1 - \lambda\phi_t^2 + \lambda\phi_r^2). \quad (26)$$

The type of this partial differential equation is determined by the discriminant

$$\Delta = \frac{1}{4}(\mathcal{B}^2 - 4\mathcal{A}\mathcal{C}) = 1 - \lambda\phi_t^2 + \lambda\phi_r^2. \quad (27)$$

For $\Delta > 0$ the equation is hyperbolic, for $\Delta = 0$ parabolic, while for $\Delta < 0$ elliptic. The DBI theory represents a special case. Requiring the Lagrangian density to be real results in the constraint (19), which excludes the possibility $\Delta < 0$. We can again estimate the distance r at which eq. (10) changes type if \mathcal{A} , \mathcal{B} , \mathcal{C} are evaluated for the configuration (3). For both values of δ_2 , the discriminant (27) may vanish when the wavepacket approaches a region in which r is approximately given by eq. (4) [6].

4. NUMERICAL METHOD

The numerical integration of the equations of motion is achieved through the implementation of a variant of the leap-frog scheme. We have found that the most efficient form of the equations is given by eqs. (6), (20). The discretized version that we employ is

$$\frac{\Delta r}{\Delta t} r_i^2 \left[G(U_i^{j+1}, V_i^{j+1}) - G(U_i^{j-1}, V_i^{j-1}) \right] = r_{i+1}^2 F(U_{i+1}^j, V_{i+1}^j) - r_{i-1}^2 F(U_{i-1}^j, V_{i-1}^j), \quad (28)$$

with $U = \phi_t$, $V = \phi_r$. The functions F and G are $F(U, V) = U(1 - \lambda U^2 + \lambda V^2)$, $G(U, V) = V(1 - \lambda U^2 + \lambda V^2)$ for the first model and $F(U, V) = U(1 - \lambda U^2 + \lambda V^2)^{-1/2}$, $G(U, V) = V(1 - \lambda U^2 + \lambda V^2)^{-1/2}$ for the second. The index j determines the discretized values of the time coordinate t , while the index i the discretized values of the radial coordinate r . The above equation must be complemented by an equation that enforces the condition $\partial\phi_t/\partial r = \partial\phi_r/\partial t$. Its discretized version is

$$U_{i+1}^j - U_{i-1}^j = \frac{\Delta r}{\Delta t} (V_i^{j+1} - V_i^{j-1}). \quad (29)$$

In practice, we solve eq. (29) for V_i^{j+1} , which we then substitute in eq. (28). The solution of the resulting algebraic equation leads to the determination of U_i^{j+1} in terms of known values at earlier times. The boundary conditions at the ends of the radial interval are not of high importance, as our analysis is restricted to time intervals during which the field is negligible there.

The above scheme provides an accurate description of the evolution of the field configuration, starting from an initial condition given by eq. (3) with $r_0 \gg r_* \gg L_*$. The initial stage is simple, as the equation of motion is essentially the wave equation. The evolution consists mainly of the displacement of the peak of the wavepacket towards smaller values of r , with an increase of its amplitude. The role of the higher-derivative terms becomes important during the later stages, when the wavepacket approaches the classicalization radius r_* . The most problematic aspect for our analysis is that continuous real solutions may cease to exist at some stage of the evolution. There are three reasons for this behavior:

- At some stage the solution develops a shock front. From this point on, the numerical integration cannot be continued, as the evolution of the shock depends on additional physical assumptions about its nature. The

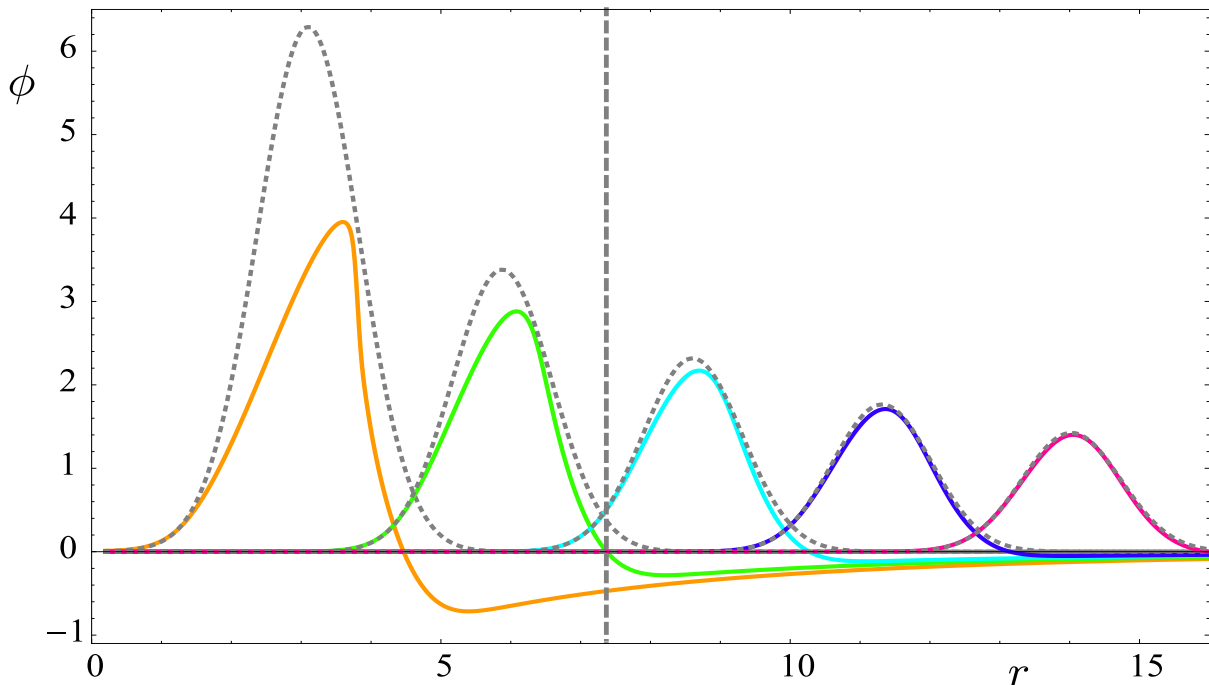


FIG. 1: The nonlinear wavepacket (solid lines) vs. the linear wavepacket (dotted lines), in the context of the DBI theory, described by eq. (16), with $\delta_2 = 1$, $L_* = 1$. The initial wavepacket has $A = 20$, $a = 1$. The vertical dashed line denotes the classicalization radius.

equation of motion becomes singular at the location of the shock and the resulting discontinuities in the field configuration, or its derivatives, cannot be determined without extra input. We do not attempt to impose additional conditions, so as to continue the integration, for two reasons: Firstly, our intuition on the physical properties of this system is limited; secondly, the scattering properties of the solution can be established already before the appearance of the shock front. We also mention at this point that the numerical solution is slightly better behaved near the shock front, if one employs the quantities F and G , appearing in eqs. (28), (29), as independent variables, instead of U and V . The reformulation of the system (28), (29) is straightforward. Our results have been obtained and cross-checked through both formulations.

- At some time a real solution ceases to exist within a certain range of r . This possibility is already apparent for static solutions of the equations of motion. For $\phi_t = 0$, eq. (6) becomes

$$\phi_r(1 + \lambda\phi_r^2) = \frac{c}{r^2}, \quad (30)$$

with c a constant of integration. In order to obtain a localized configuration of finite energy, we must assume that ϕ_r approaches c/r^2 for large r . The solution with this asymptotic behavior extends down to $r = 0$ (where it diverges) for $\lambda > 0$, while it becomes complex at some $r \neq 0$ for $\lambda < 0$. For the DBI action, eq. (20) becomes

$$\frac{\phi_r}{\sqrt{1 + \lambda\phi_r^2}} = \frac{c}{r^2}, \quad (31)$$

which gives $\phi_r = c/\sqrt{r^4 - \lambda c^2}$. For $\lambda < 0$ the solution is real for all r , while for $\lambda > 0$ it becomes imaginary for $r < \lambda^{1/4}|c|^{1/2}$. Similar behavior may occur in the solutions of the full dynamical problem. However, it is difficult to predict, or even classify, the various cases, as no analytical treatment of these partial differential equations is available. In the following section we describe cases in which the time-dependent solution ceases to be real in certain ranges of r . In the final section we discuss the origin of this behavior.

- The third type of complication occurs at the time when the partial differential equation switches type within a range of r . This change is indicated by the discriminant Δ approaching zero from positive values. For $\Delta < 0$ the equation becomes elliptic and its solution requires (Dirichlet or Neumann) boundary conditions on a closed

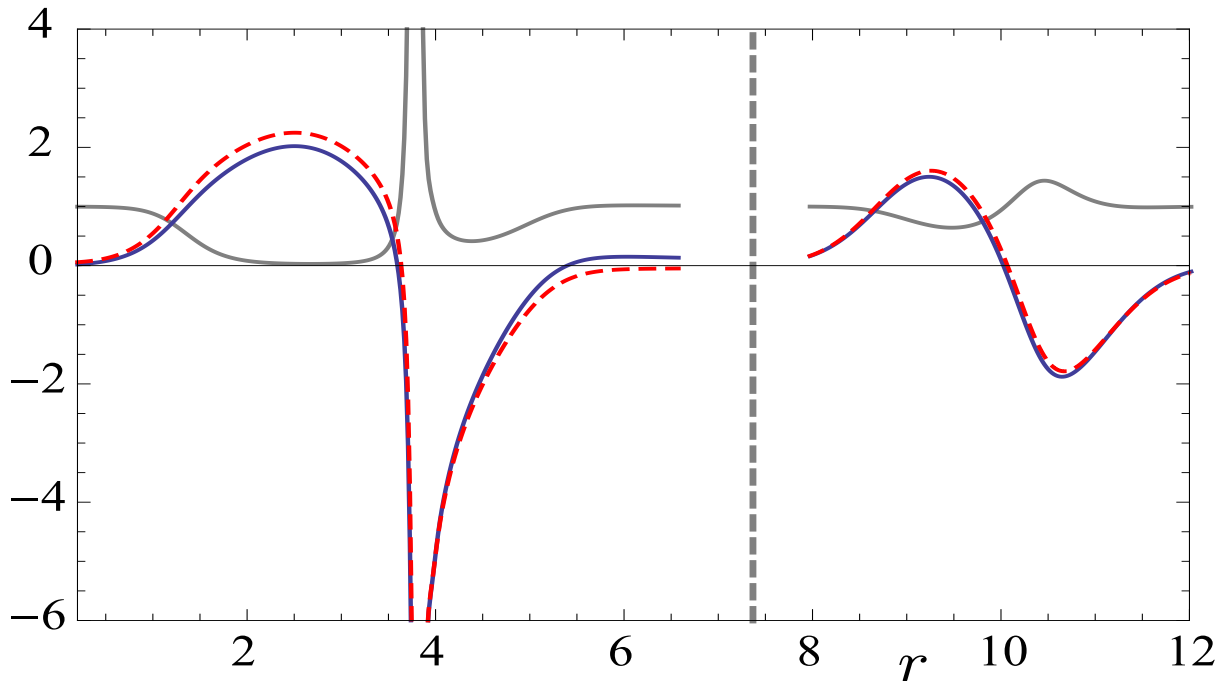


FIG. 2: The derivatives ϕ_t (dashed) and ϕ_r (solid) of the nonlinear field, and the discriminant Δ of eq. (27) (solid grey), at two different times, before and after the crossing of the classicalization radius. The model is the same as in fig. 1. The vertical dashed line denotes the classicalization radius.

contour around the region of interest. Unfortunately, the scattering problem that we are considering cannot provide such conditions, as it is set up through Cauchy boundary conditions at the initial time. For $\Delta < 0$ the coordinate t becomes essentially spatial. Boundary conditions on a closed contour would require the values of ϕ or its derivatives at times later than the time of interest. In the standard (and rather limited) studies of partial differential equations of mixed type, the boundary conditions are imposed on appropriate boundaries so that a unique solution exists. In the case we are considering this is not possible.

The above complications indicate that the idealized scattering problem that we are considering is not always well posed mathematically. The most disturbing issue is the inability to find a solution in the range of r where the equation becomes elliptic. A reformulation of the problem is needed in order to overcome this difficulty. Despite these misgivings, a solution of the equation of motion over sufficiently long time intervals, so as to probe the region of classicalization, is possible in many cases. In the following section we present explicit examples.

5. NUMERICAL RESULTS

We have found that the solutions with the most regular behavior are obtained in the context of the DBI model, described by the Lagrangian (16), with $\delta_2 = 1$ and, therefore, $\lambda > 0$. In fig. 1 we depict the solution of the equation of motion at various times. We have normalized all dimensionful quantities with respect to the fundamental scale of the theory. This is equivalent to setting $L_* = 1$. We have considered an initial spherical wavepacket with a width equal to the fundamental scale ($a = 1$), as the preparation of a narrower configuration would presuppose that scales below L_* can be probed. The amplitude of the configuration must be much larger than 1 in order for the classicalization radius to satisfy $r_* \gg L_*$. We use $A = 20$. The solid lines denote the nonlinear field $\phi(t, r)$ resulting from the integration of eq. (6). The dotted lines denote the evolution of the initial configuration $\phi_0(t, r)$ if the nonlinear terms are neglected ($\lambda = 0$). In this case the equation of motion is the wave equation in spherical coordinates, and eq. (3) provides its exact solution.

As expected, the nonlinear and linear field configurations coincide at early times, when the peak of the wavepacket is located at distances much larger than r_* . The nonlinear configuration is subject to visible deformations when the peak approaches r_* . The deformations become significant when the wavepacket crosses inside the classicalization radius. The final configuration in fig. 1 depicts a wavepacket whose front end is located at distances below $L_* = 1$. Its

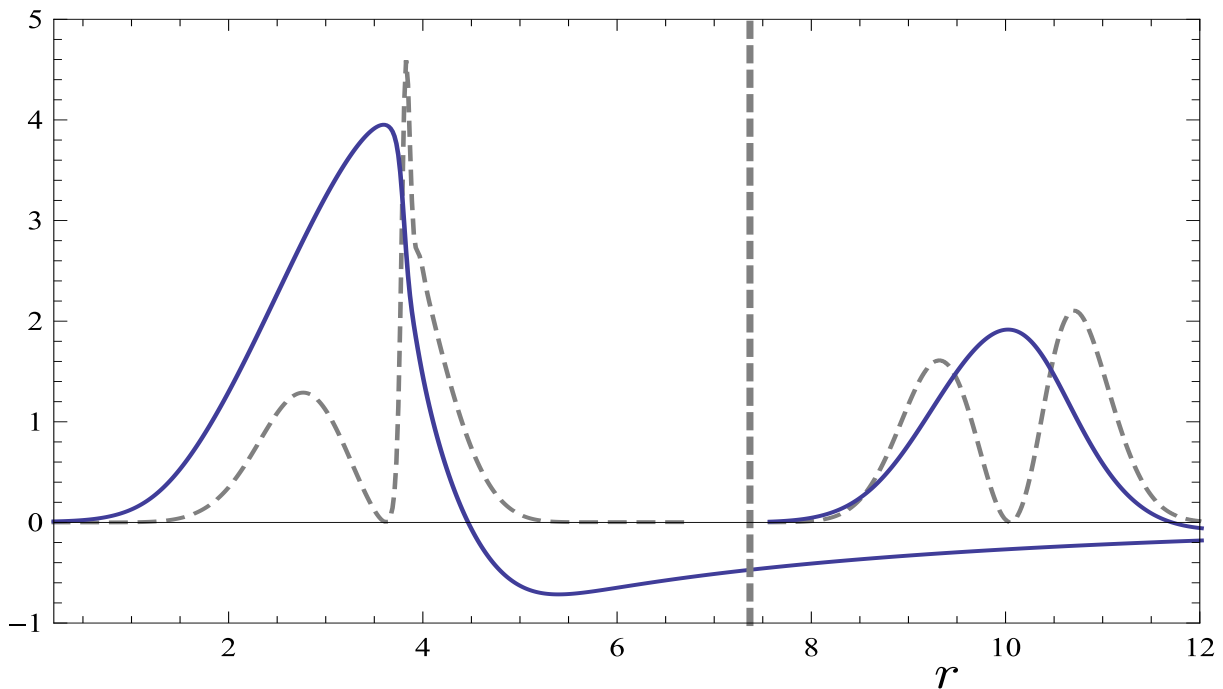


FIG. 3: The nonlinear field ϕ (solid) and the product $4\pi r^2 \rho$, with ρ the energy density (dashed). The model is the same as in fig. 1. The vertical dashed line denotes the classicalization radius. The energy density is multiplied by 5×10^{-4} .

height is reduced significantly in relation to the linear configuration. Its back end develops a long tail that extends far beyond the classicalization radius. The last important feature of the configuration is that the part behind the peak is very steep, essentially vertical. This indicates the appearance of a shock front, where the field derivatives become singular.

In fig. 2 we display some characteristics of the solution before and after the r_* -crossing. The dashed and solid lines that almost coincide depict the derivatives ϕ_t and ϕ_r , respectively. The grey solid line depicts the discriminant Δ of eq. (18), given by eq. (27). The form of the field at early times, seen on the right of the vertical dashed line marking the classicalization radius, is typical of an incoming spherical wavepacket. The derivatives ϕ_t , ϕ_r are almost equal, while the discriminant deviates only slightly from 1. The late-time configuration, located within the classicalization radius, has a significantly different form. Within a small r -interval around the shock front, the radial derivative ϕ_r becomes negative, with an absolute value that becomes very large. The time-derivative ϕ_t has a similar form. At large r , both ϕ_t , ϕ_r approach zero, having opposite signs. This is an important feature that we shall discuss in detail below. The discriminant displays three types of behavior: In the regions where ϕ_t , ϕ_r are small, it takes values very close to 1, as the nonlinear terms in the equation of motion are subleading. At the location of the shock front, it becomes very large. In the remaining regions it approaches zero. This last feature is clearly visible in the region $2 \lesssim r \lesssim 3.5$. It indicates that the partial differential equation (18) becomes essentially parabolic within this region. For wavepackets with larger amplitude A , the transitions in the values of Δ between 0, 1 and very large values at the shock front become very sharp.

In fig. 3 we display some additional features of the field configuration before and after the r_* -crossing. The solid lines depict the field. The late-time configuration is characterized by a very long tail that extends well beyond the classicalization radius. The dashed lines depict the product $4\pi r^2 \rho$, with the energy density ρ given by eq. (22). The total energy of the configuration, corresponding to the area below the dashed lines, remains constant during the evolution. Actually, the conservation of the energy is one of the criteria that we employ in order to estimate the accuracy of the numerical integration. For both configurations depicted in fig. 3, the energy is distributed roughly equally between the front and back end of the wavepacket. When the shock front develops, the energy density becomes strongly peaked at its location. The long tail of the late-time configuration carries very little energy, as both ϕ_t , ϕ_r are very small there.

The properties of the tail appearing at late times in figs. 1–3 are the main observable consequence of the classicalization scenario. In the region within which the tail develops, the equation of motion is essentially the wave equation, as ϕ_t , ϕ_r are very small and the nonlinear corrections negligible. For this reason we expect that the field can be

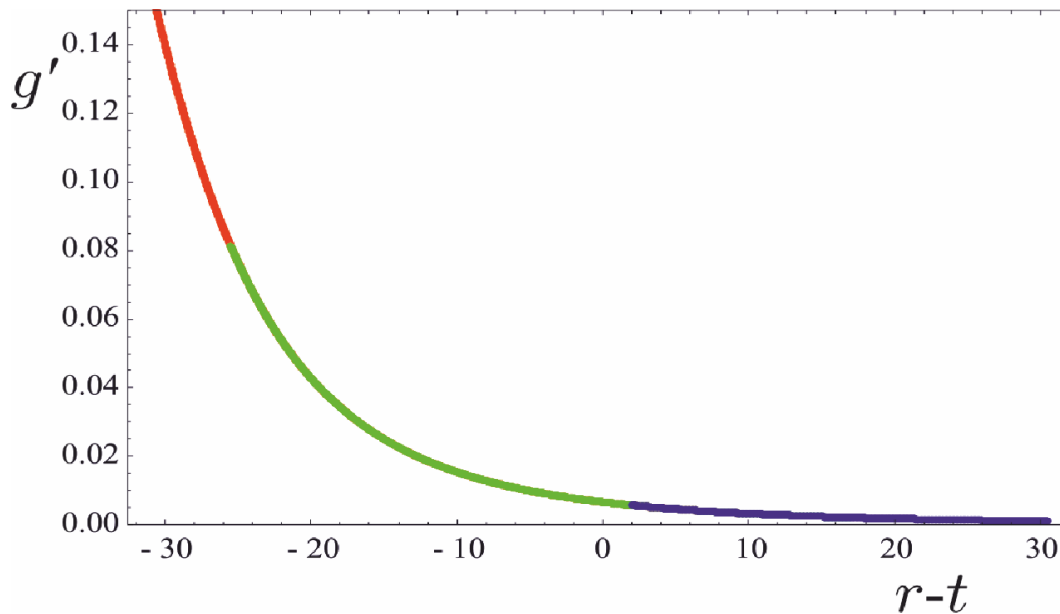


FIG. 4: The derivative of the function $g(r-t)$ appearing in the asymptotic form of the field (eq. (32)). The model is the same as in fig. 1.

expressed as

$$\phi(t, r) = \frac{1}{r} [f(r+t) + g(r-t)]. \quad (32)$$

The unknown functions f and g can be determined from our numerical solution through the relations

$$f'(r+t) = \frac{1}{2} [r(\phi_r(t, r) + \phi_t(t, r)) + \phi(t, r)] \quad (33)$$

$$g'(r-t) = \frac{1}{2} [r(\phi_r(t, r) - \phi_t(t, r)) + \phi(t, r)], \quad (34)$$

where the primes denote derivatives with respect to the arguments. Our results indicate that to a very good accuracy $f'(r+t) = 0$, so that we can set consistently $f(r+t) = 0$ in eq. (32). Thus the tail of the field represents an outgoing configuration, which can be interpreted as a result of the scattering of the initial incoming wavepacket. We have also determined the form of the derivative of the function $g(r+t)$, by using data at different times. The result is depicted in fig. 4, where we have indicated parts of the curve computed at different times. They all form a continuous curve, with overlapping parts that are consistent with each other to a high accuracy. Within the tail, the field ϕ is a monotonically increasing function of $r+t$, starting from negative values and vanishing for large arguments. We have performed various fits of the curve depicted in fig. 4. The best one involves a combination of two terms of the form $A/(r-t+c)^n$, with A , c , n determined by the data. Even though the data do not provide a unique answer, we find that a combination of powers with $n \sim 3-5$ gives the best fit. This behavior is consistent with the analytical results of ref. [2] for the theory described by the Lagrangian density (1).

The DBI model with $\delta_2 = -1$ and $\lambda < 0$, with an initial condition given by eq. (3), displays the second of the problems we described at the end of the previous section. A real solution over the whole range of r cannot be found after a certain time during the very early stages of the evolution. The problem appears near the extrema of ϕ_r , where $1 + \lambda\phi_r^2$ vanishes. It is important to note that this term multiplies ϕ_{tt} if the equation of motion is written in the form (18). In the following section we investigate the origin of this behavior.

We next turn to the quartic model described by the Lagrangian (1). The most regular behavior is obtained for the model with $\delta_1 = -1$ and, therefore, $\lambda < 0$. The evolution of the initial wavepacket is similar to that shown in fig. 1. In figs. 5, 6 we depict the solution at some early stage and at the latest time at which the solution is hyperbolic over the whole range of r ($\Delta > 0$ everywhere). The form of the solution is very similar to that depicted in figs. 2, 3 for the DBI model. In contrast to the DBI model with $\lambda > 0$, the evolution at later times takes the system into the region where the equation of motion becomes elliptic ($\Delta < 0$) within a certain r -interval. As we explained in the previous

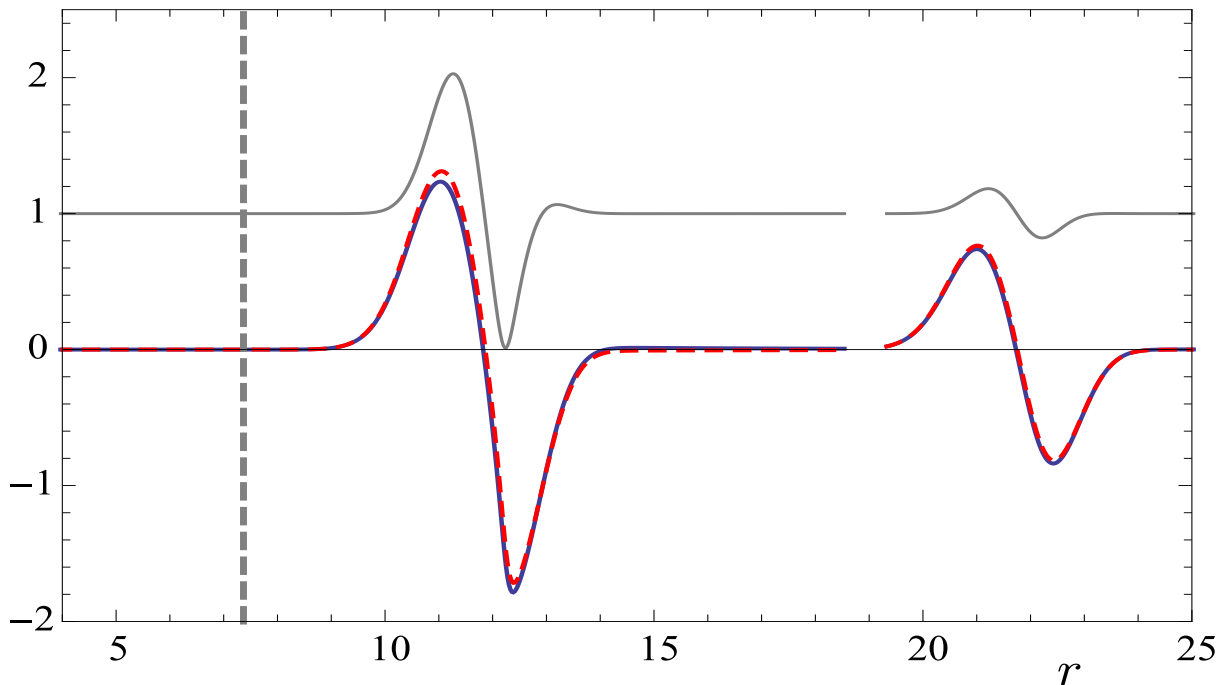


FIG. 5: The derivatives ϕ_t (dashed) and ϕ_r (solid) of the nonlinear field, and the discriminant Δ of eq. (15) (solid grey), at two different times, in the context of the quartic theory, described by eq. (1), with $\delta_1 = -1$, $L_* = 1$. The initial wavepacket has $A = 20$, $a = 1$. The vertical dashed line denotes the classicalization radius.

section, the boundary conditions provided by the scattering problem are not appropriate for the determination of a unique solution of the equation of motion when it becomes of mixed type (elliptic within a certain region, while staying hyperbolic in other regions). We find that instabilities tend to develop during the numerical integration when Δ becomes negative. The accuracy of the integration remains high during an initial stage at which the equation of motion is of mixed type. It diminishes gradually, until the numerical solution becomes unreliable at some time before the wavepacket reaches the classicalization radius (denoted by the vertical dashed line in figs. 5,6).

Despite the above limitations, some useful information can be extracted from our solution. It is obvious from fig. 5 that the evolution of the wavepacket is similar to that in the DBI case with $\lambda > 0$. The rear of the wavepacket becomes steeper and a shock front starts developing. This is indicated by ϕ_r becoming more negative. In the same time, a long tail is clearly visible at large values of r in fig. 6. The solid line in fig. 5 represents the discriminant Δ given by eq. (15). We have depicted the form of the wavepacket at the time when Δ first reaches zero at a certain value of r .

Finally, the quartic model with $\lambda > 0$ displays the same behavior as the DBI model with $\lambda < 0$. A real solution ceases to exist at some early stage in the evolution, at the time when the coefficient $1 - 3\lambda\phi_t^2 + \lambda\phi_r^2$ of ϕ_{tt} in the equation of motion (5) vanishes.

6. DISCUSSION AND CONCLUSIONS

Despite some inherent problematic issues, our analysis of the idealized scattering process with exact spherical symmetry has provided concrete evidence for certain features of the classicalization scenario:

- The classicalization radius of eq. (4) sets the scale for the onset of significant deformations of a collapsing classical configuration with large energy concentration in a central region. This behavior is consistent with the expectations of refs. [1–4].
- The equation of motion is a quasilinear partial differential equation of hyperbolic type at early times. At distances comparable to the classicalization radius, the nonlinearities become significant and can change the equation type. We discussed in detail an example in which the equation becomes essentially parabolic in certain regions of space. This is consistent with the analysis of ref. [6]. We also discussed an example in which the

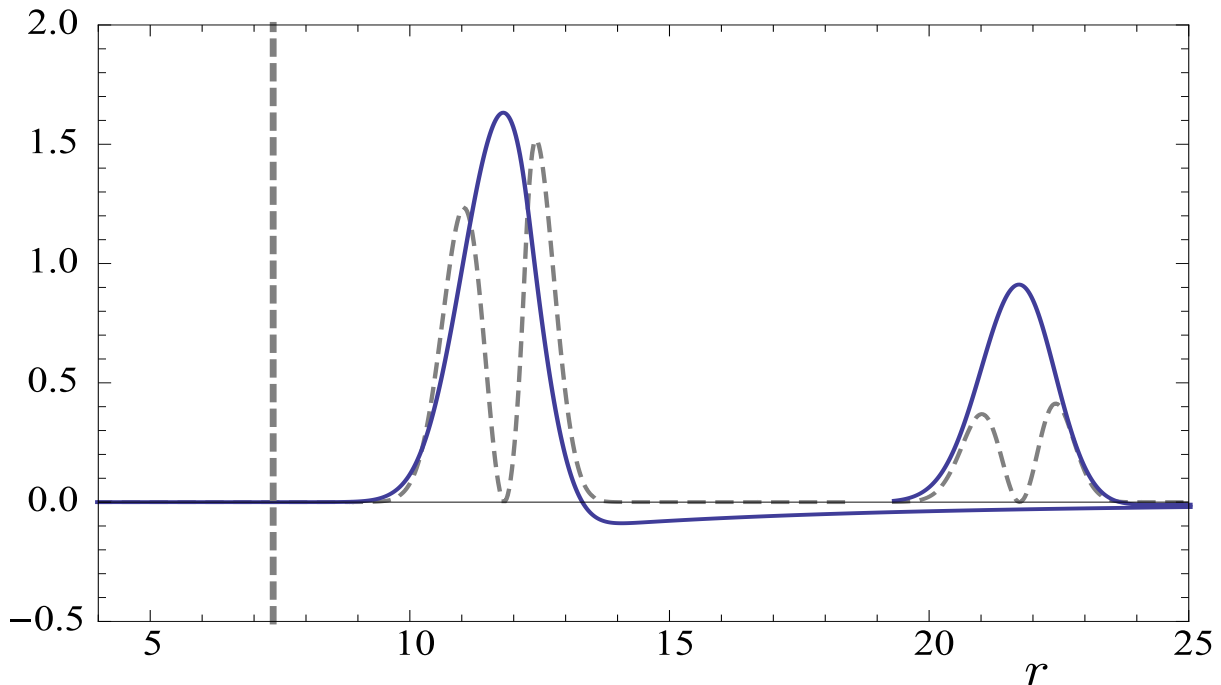


FIG. 6: The nonlinear field ϕ (solid) and the product $4\pi r^2 \rho$, with ρ the energy density (dashed). The model is the same as in fig. 5. The vertical dashed line denotes the classicalization radius. The energy density is multiplied by 5×10^{-4} .

evolution makes the equation elliptic within a certain region. However, a real solution cannot be found at late times within the elliptic region. It seems likely that the initial conditions of the scattering process are not appropriate for the solution of the mixed type equation.

- Shock fronts develop during the scattering process at distances comparable to the classicalization radius, consistently with the expectations of ref. [6].
- The most important observable feature of the classicalization process is the creation of an outgoing field configuration that extends far beyond the classicalization radius. This feature develops before the deformed wavepacket reaches distances of the order of the fundamental scale L_* .

Our study has also revealed several novel issues related to classicalization:

- Our numerical analysis in the context of the DBI model indicates that the collapsing wavepacket can approach distances of the order of the fundamental scale L_* before strong scattering appears. However, this could be a special feature of the DBI model. As we have seen, the equation of motion cannot become elliptic in this system, so that free propagation of wavelike configurations is not eliminated.
- The scattering resulting from the early stages of the classicalization process seems to be minimal within our analysis. The tail of the field configuration carries a negligible amount of energy because the corresponding modes are extremely soft. Within the DBI model, the bulk of the energy stored in the initial wavepacket can end up within a region of space with length scale comparable to L_* . Similarly to the previous point, this behavior may be a special feature of the DBI model.
- Our analysis does not provide evidence for the creation and subsequent decay of a quasistatic configuration that could be identified with the classicalon of refs. [1–4]. Instead, the classicalization scenario seems to be a fully dynamical process, whose defining feature is that it is characterized by a scale different from the naive length scale deduced from the higher-derivative terms in the Lagrangian density. A curious fact is that the static classicalons seems to exist in the two cases (quartic model with $\lambda > 0$ and DBI model with $\lambda < 0$) in which a dynamical solution ceases to exist at an early stage of the evolution.
- The most unexpected issue that emerged in our analysis is that the scattering problem may not have real solutions over the whole space within the context of the higher-derivative theories that support classicalization.

In view of the above conclusions, a few more comments are in order concerning the accuracy of our analysis and the nature of the solutions. We have found that, in several of the versions of the equation of motion that we studied, an initial configuration representing a collapsing spherical wavepacket cannot evolve beyond a certain time. A real solution of the equation of motion ceases to exist for the initial condition of eqs. (3),(9). It is always possible that the inability to find a solution may be caused by the scheme we employed for the numerical solution of the equation of motion. For this reason, apart from the explicit leap-frog method we described in section 4, we reproduced our results through a second integration method, based on an implicit Crank-Nicolson scheme. The agreement is very good in the regions in which a solution exists, while both methods indicate the absence of a real solution in the same ranges of t and r .

In order to obtain a more intuitive understanding of the type of solutions that emerged in our analysis, we find it instructive to consider simplified toy models that display similar behavior. In section 4, we discussed the static (classicalon) solutions, some of which do not exist over the entire range of r . Time-dependent analytical solutions are more difficult to derive in a field-theoretical context. However, simple toy models can be solved explicitly. The simplest one is a harmonic oscillator of unit mass and non-standard kinetic terms.

The analogue of the quartic model we discussed in section 2 is described by a Lagrangian

$$L = \frac{1}{2}\dot{x}^2 - \frac{1}{4}\delta\xi\dot{x}^4 - \frac{1}{2}\omega^2x^2, \quad (35)$$

with $\delta = \pm 1$ and $\xi > 0$. The equation of motion is

$$(1 - 3\delta\xi\dot{x}^2)\ddot{x} + \omega^2x = 0. \quad (36)$$

Its first integral is the conserved energy

$$E = \frac{1}{2}\dot{x}^2 - \frac{3}{4}\delta\xi\dot{x}^4 + \frac{1}{2}\omega^2x^2 = \frac{1}{2}\omega^2x_0^2, \quad (37)$$

where we have assumed that initially the particle is at rest at $x = x_0$. For this initial condition, the above equation gives

$$\dot{x}^2 = \frac{1 - \sqrt{1 - 6\delta\xi\omega^2(x_0^2 - x^2)}}{3\delta\xi}. \quad (38)$$

For $\delta = -1$ a solution exists at all times, describing a particle oscillating around the minimum of the potential at $x = 0$. For $\delta = 1$ a real oscillating solution exists at all times if $x_0^2 < (6\xi\omega^2)^{-1}$. However, for $x_0^2 > (6\xi\omega^2)^{-1}$ only a complex solution exists below the point with $x^2 = x_0^2 - (6\xi\omega^2)^{-1}$. This is reached at the time when the coefficient of \ddot{x} in eq. (36) vanishes. We observed very similar behavior in the solutions described in section 5.

The crucial property of the Lagrangian (35) with $\delta = 1$ is that the kinetic part of the corresponding energy, given by eq. (37), is bounded from above when considered as a function of \dot{x} . If the evolution starts at a sufficiently large value of x , the initial potential energy can be larger than the maximal possible kinetic energy. As a result, the conservation of energy cannot be satisfied at some point during the evolution of the particle towards the minimum of the potential, and a real solution ceases to exist. The maximal value of the kinetic energy is obtained for $1 - 3\xi\dot{x}^2 = 0$. This explains why a real solution does not exist beyond the time at which the coefficient of \ddot{x} in eq. (36) vanishes. It is also interesting to consider the momentum conjugate to x , given by $p = \dot{x}(1 - \xi\dot{x}^2)$. This expression has a local maximum for $\dot{x}^2 = 1/(3\xi)$. The function $\dot{x} = \dot{x}(p)$ is multivalued in a range of p around the origin. The quantization of this model may pose difficulties.

The field theoretical model of eq. (1) with $\delta_1 = 1$ and $\lambda > 0$ has very similar features with the toy model. The energy density of eq. (8) has a maximum as a function of ϕ_t at the point at which the coefficient of ϕ_{tt} in eq. (5) vanishes. This occurs at the time at which $1 - 3\lambda\phi_t^2 + \lambda\phi_r^2$ becomes zero for a certain value of r and the numerical integration stops converging. The origin of the problem is now clear: The energy cannot be conserved beyond this point and a real solution does not exist any more. The momentum density conjugate to ϕ , given by $\pi = \phi_t(1 - \phi_t^2 + \phi_r^2)$, has a maximum as a function of ϕ_t when $1 - 3\lambda\phi_t^2 + \lambda\phi_r^2 = 0$. Similarly to the toy model, the quantization of such a theory is not straightforward and may be problematic. It must be pointed out that the static classicalon exists as a solution over the whole space only for $\delta_1 = 1$, as can be seen from eq. (30). The model with $\delta_1 = -1$ has a better-behaved dynamical solution, but the static classicalon exists only within a limited range of r .

The analogue of the DBI model of section 3 is described by a Lagrangian

$$L = -\frac{1}{\delta\xi}\sqrt{1 - \delta\xi\dot{x}^2} - \frac{1}{2}\omega^2x^2, \quad (39)$$

with $\delta = \pm 1$ and $\xi > 0$. The equation of motion is

$$\ddot{x} + (1 - \delta \xi \dot{x}^2)^{3/2} \omega^2 x = 0, \quad (40)$$

and the conserved energy

$$E = \frac{1}{\delta \xi \sqrt{1 - \delta \xi \dot{x}^2}} + \frac{1}{2} \omega^2 x^2 = \frac{1}{\delta \xi} + \frac{1}{2} \omega^2 x_0^2, \quad (41)$$

where we have assumed that initially the particle is at rest at $x = x_0$. The above equation can be rewritten as

$$\frac{1}{\sqrt{1 - \delta \xi \dot{x}^2}} - 1 = \frac{1}{2} \delta \xi \omega^2 (x_0^2 - x^2). \quad (42)$$

For $\delta = 1$ a solution exists at all times, describing a relativistic particle oscillating around the minimum of the potential at $x = 0$. We observed very similar behavior in the solution depicted in figs. 1-3, which exists at all times up to the formation of the shock front.

For $\delta = -1$ a real oscillating solution always exists if $x_0^2 < (2\xi\omega^2)^{-1}$. However, for $x_0^2 > (2\xi\omega^2)^{-1}$ a real solution ceases to exist when the particle reaches the point with $x^2 = x_0^2 - (2\xi\omega^2)^{-1}$, at which \dot{x} diverges. The origin of the problem can again be traced to the fact that the kinetic energy in eq. (41) is bounded from above when considered as a function of \dot{x} . The maximum occurs for $\dot{x} \rightarrow \infty$. The conjugate momentum $p = \dot{x}/\sqrt{1 + \xi\dot{x}^2}$ also has a maximal value obtained for $\dot{x} \rightarrow \infty$. The corresponding field theory is the DBI model of eq. (16) with $\delta_2 = -1$ and $\lambda < 0$. The partial derivative with respect to ϕ_t of the energy density of eq. (22) vanishes at the point where $1 + \lambda\phi_r^2$, the coefficient of ϕ_{tt} in eq. (18), becomes zero. The partial derivative with respect to ϕ_t of the momentum density $\pi = \phi_t/\sqrt{1 - \lambda\phi_t^2 + \lambda\phi_r^2}$ also vanishes at the same point. These properties are responsible for the absence of a real solution of eq. (18) beyond this point, as the classical evolution cannot conserve the total energy of the system. We point out that the static classicalon exists as a solution over the whole space only in the case with $\delta_2 = -1$ and $\lambda < 0$, as can be seen from eq. (31).

In summary, our analysis has confirmed the existence of nontrivial physical behavior at distances much larger than the fundamental length scale in theories that support classicalization. It has also revealed some peculiar features of certain underlying theories, which may lead to the absence of real solutions of the classical equations of motion and difficulties with quantization. It remains to be seen whether the breakdown of the classical evolution is a pathology of such theories, or whether it signals the transition to a regime in which the role of quantum physics is dominant. The one-dimensional toy models we considered in this section may provide crucial intuition on this issue.

Acknowledgments

We would like to thank N. Brouzakis for collaboration during the early stages of this work and many useful discussions. We would also like to thank G. Dvali for useful discussions. The research of J. R. and N. T. was supported in part by the ITN network ‘‘UNILHC’’ (PITN-GA-2009-237920).

-
- [1] G. Dvali, G. F. Giudice, C. Gomez and A. Kehagias, arXiv:1010.1415 [hep-ph].
 - [2] G. Dvali and D. Pirtskhalava, Phys. Lett. B **699** (2011) 78 [arXiv:1011.0114 [hep-ph]].
 - [3] G. Dvali, arXiv:1101.2661 [hep-th].
 - [4] G. Dvali, C. Gomez and A. Kehagias, JHEP **1111** (2011) 070 [arXiv:1103.5963 [hep-th]].
 - [5] C. Grojean and R. S. Gupta, arXiv:1110.5317 [hep-ph].
 - [6] N. Brouzakis, J. Rizos and N. Tetradis, arXiv:1109.6174 [hep-th].